Bivariate multifractal analysis for non-homogenous point processes, with application to geospatial data

Janka Lengyel
Université de Lyon, ENS de Lyon
CNRS, Lab. de Physique, Lyon (FR)
Univ Gustave Eiffel, Ecole des Ponts
LVMT, Marne-la-Vallée (FR)
janka.lengyel@ens-lyon.fr

Stéphane Roux
Université de Lyon, ENS de Lyon
CNRS, Lab. de Physique, Lyon (FR)
stephane.roux@ens-lyon.fr

Ptashanna Thiraux
Université de Lyon, ENS de Lyon
CNRS, Lab. de Physique, Lyon (FR)
ptashanna.thiraux@ens-lyon.fr

Patrice Abry
Université de Lyon, ENS de Lyon
CNRS, Lab. de Physique, Lyon (FR)
patrice.abry@ens-lyon.fr

Olivier Bonin
Univ Gustave Eiffel, Ecole des Ponts
LVMT, Marne-la-Vallée (FR)
olivier.bonin@univ-eiffel.fr

Stéphane Jaffard
Univ Paris Est Creteil, CNRS
LAMA, UMR 8050, Créteil (FR)
stephane.jaffard@u-pec.fr

***Abstract*—Multifractal analysis has become an important procedure for estimating local regularities in experimental data. However, while univariate multifractal analysis is well-established, how cross-dependencies of regularities fluctuate amongst signal components is less often addressed. Further, multifractal analysis is now thoroughly outlined for fields defined everywhere on raster-like data structures. Still, it is less well suited for analyzing processes that exist only on restricted and partial supports, possibly with heterogeneous densities. These two issues, critical for a relevant application of multifractal analysis to geospatial data, are addressed here by proposing an original point process-oriented bivariate multifractal analysis. The relevance of the proposed procedure is illustrated at work on synthetic data constructed by combining homogenous and non-homogeneous point processes with multifractal textures. Illustration on real-world geospatial data is also provided.**

***Index Terms*—Point processes, bivariate multifractal analysis, regularity cross-dependencies, geospatial data**

I. Introduction

Context. In many applications of geography and urban science, several phenomena are measured and analyzed jointly in several points of the same territory, taking the form of *multivariate* data. Furthermore, in such investigations, the *support* or the spatial distribution of the data, i.e., the locations where the phenomena are measured, is often neither a homogeneous compact set nor a 2D raster grid. Hence, their modeling often entails (two-dimensional) point processes with possibly non-homogenous densities. Finally, the concept of *scale-free* spatial dynamics and thus of multifractal analysis and modeling has already been put forward as relevant for urban analysis [1]–[5]. Nevertheless, the above three aspects of geographical data - multidimensionality, cross-multifractality, and non-homogeneity - have rarely been studied jointly, an issue at the heart of the present work.

Related work. Multifractal analysis, which describes the properties of the fluctuations of local regularity in time or space, is a well-known signal processing tool successfully tested in numerous real-world applications [6]. However, it mainly remained univariate in spirit: components of the data were analyzed independently, one after the other. The extension of multifractal analysis to bivariate settings was introduced in physics in [7] and formalized mathematically in [8]. Recently, a theoretically well-grounded and practically robust multivariate multifractal framework has been devised [9]–[11]. It permits the assessment of cross-dependencies in fluctuations of local regularities amongst the different components of the data [12]. The proposed framework applies only to classical *images* so far, that is, to 2D raster grids that are everywhere well-defined. Independently, spatial statistical analysis [13] considers many geospatial datasets to be marked point processes that can be accordingly characterized by their ("point") locations and one or more attached quantities or "marks" (e.g., demographic variables). Finally, in geographical data science, an original framework for univariate multifractal analysis was developed [2]–[4]. It relies on the design of specific multiscale quantities, the essential ingredients for scale-free analysis, which are customized to be beneficial for studying non-homogeneous point processes.

Goals, contributions, and outline. Building upon this research, the present work aims to construct an original bivariate multifractal analysis framework that is well-suited to the analysis of non-homogeneous point patterns and to show its relevance to the analysis of actual geospatial data. To that end, Section II briefly recalls classical multifractal analyses. Section III develops the core contribution of this article: It introduces a novel multiscale quantity suited to point processes and defines local bivariate multifractal analysis. The relevance of the proposed tool is illustrated on synthetic data constructed from multifractal measures restricted to three types of point patterns: a homogeneous grid and two non-homogenous Sierpinski carpets (see Section IV). Finally, the potential benefits of using such tools on real-world geospatial data are assessed in Section V. The underlying computational methodology - devised by the authors - is also available as an open-source python package `LomPy`, which can be accessed at [14].

II. Classical multifractal analysis

Multifractal analysis characterizes the fluctuations of *local regularity* in time or space of a process κ. Different pointwise regularity exponents can be used, the most widespread being the Hölder exponent $h(x_0)$, which is relevant for locally bounded processes. It is defined as the largest α such that there exist, in a neighborhood of x_0, a constant $C > 0$ and a polynomial P (of order less than α) satisfying $|\kappa(x_0 - r) - P(x_0 - r)| < C|r|^{\alpha}$.

A. Multifractal spectrum and formalism

Based on a local regularity measure, multifractal analysis provides global and geometrical information related to the structure of the fluctuations in local regularity $h(x)$. This information is classically shown via the multifractal spectrum $D(h)$, defined as the collection of Hausdorff dimensions ($\dim_H$) of the sets of points x, where $h(x)$ takes the value h:

$$D(h) = \dim_H \left\{ x \text{ such that } h(x) = h \right\}.$$

The practical estimation of the multifractal spectrum relies on studying the evolution along scales of the statistics of well-chosen multiscale quantities. Defined initially as increments, it has abundantly been shown that wavelet coefficients [15] or some non-linear transformations of these [16] constitute more suitable choices for multifractal analysis.

Let $T(x, r)$ denote the multiscale quantities computed at location x and scale r. A process κ is said to possess scale-free characteristics if, for some statistical orders q, the space averages of $|T(x, r)|^q$ in a fixed scale display power law behaviors as functions of scale r

$$S_q(r) = \mathbb{E}\{|T(x,r)|^q\} = \lim_{N \to +\infty} \sum_{x=1}^{N} |T(x,r)|^q \sim F_q |r|^{\zeta_q}$$

where N is the total number of points x that $T(x, r)$ is computed, and $\mathbb{E}$ refers to the global space average. The scaling exponents ζ_q are related by a Legendre transform to the multifractal spectrum $D(h) \leq \min_q(qH - \zeta_q)$, with equality for large classes of models.

When ζ_q is smooth around 0, a Taylor expansion of $\zeta_q = \sum_{p \leq 1} c_p \frac{q^p}{p!}$ shows that the cumulants of the logarithm of the multiscale quantities behave linearly with respect to scales r, yielding for the two first orders:

$$\begin{aligned} C_1(r) &= \mathbb{E}\{log|T(x,r)|\} = c_1 \log(|r|) + d_1 \\ C_2(r) &= \mathbb{E}\{\left(log|T(x,r)| - C_1(r)\right)^2\} = -c_2 \log(|r|) + d_2. \end{aligned}$$

This provides practitioners with a quadratic approximation of the multifractal spectrum around its maximum: $D(h) \sim 2 - \frac{(h-c_1)^2}{2c_2}$, which shows that c_1 encodes the location of the maximum of the spectrum, and $c_2 > 0$ its width. Therefore, (c_1, c_2) are often considered to be a relevant summary of the multifractal properties of the data. Often, in applications and for historical reasons, the pair (H, c_2) is used instead of (c_1, c_2), where the Hurst or self-similarity exponent $H \equiv \zeta(2)/2$ is practically very close to c_1 as $H \simeq c_1 - c_2$ and $c_2 \ll c_1$ (c_1 can be interpreted as the almost everywhere regularity of the process).

B. Bivariate extension

In a bivariate setting, local regularities are quantified independently for each component of the data, resulting in a vector of bivariate measure of local regularity: $(h_1(x), h_2(x))$. The corresponding bivariate multifractal spectrum is

$$D(h_1, h_2) = \dim_H \left\{ x \text{ such that } (h_1(x), h_2(x)) = (h_1, h_2) \right\}.$$

The overall shape of $D(h_1, h_2)$ provides information on the multifractality of each component via the two pairs of univariate parameters (H^i, c_2^i), $i = 1, 2$ as well as on the cross multifractality. Several quantities were proposed to quantify the cross-multifractality, e.g., [9]–[11]. We define in Section III a version of those quantities in the context of point processes.

III. Local and bivariate multifractal analysis for 2D point processes

The targeted extension of the standard multifractal analysis has two challenges to address. First, it must overcome the obstacle of *non-homogenous point densities*. Second, it is to accurately estimate fractal and multifractal parameters and their correlations on the *local level*, i.e. on neighborhoods of arbitrary size smaller than the extent of the observed 2D field.

A. Multiscale quantity and local weighting function

Let us start by considering the multiscale quantity defined as the average of pairwise increments of the process $\kappa(x) = \{\kappa^1(x), \kappa^2(x)\}$, i.e., in a bivariate setting with $i = 1, 2$,

$$P^i(x, r) \quad = \quad \frac{1}{N^i(x, r)} \sum_{x',\, d_{x,x'} \leq r} \kappa^i(x) - \kappa^i(x'). \qquad (1)$$

and where $N^i(x, r)$ is the number of points in a ball of radius r, centered on x and $d_{x,x'}$ is the Euclidean distance. A direct adaptation of the wavelet *p-leaders* [16] yields the following quantities

$$Q^i(x, r) \quad = \quad \sum_{\substack{x',\, d_{x,x'} \leq r \\ r' < r}} (|P^i(x', r')|^p (\frac{r}{r'})^d)^{1/p}. \qquad (2)$$

where the sum of r' is taken on a geometric sequence of scales. To perform a local analysis, we first define a local neighborhood L larger than the radius r. Second, we introduce a homogenous raster of arbitrary grid size l with points x_g, which will serve as the focal points for local estimations. Moving on, with $T^i(x, r)$ standing for each of the multiscale quantities $P^i(x, r)$ and $Q^i(x, r)$, we compute cumulants of the logarithm of the variables $\{T^1(x, r), T^2(x, r)\}$ weighted by the distance between a chosen estimation site x_g and the locations of the original point process x. The first and second order log-cumulants read, with $i = 1, 2$:

$$C_1^i(x_g, r) = \sum_x w_{x_g,x} \log |T^i(x, r)| \qquad (3)$$

$$C_2^i(x_g, r) = \sum_x w_{x_g,x} \left(\log |T^i(x, r)| - C_1^i(x_g, r)\right)^2. \qquad (4)$$

The weights are defined as $w_{x_g,x} = f(||x_g - x||/L)$, with $f(x) = 1$ if $||x|| < 1$ and 0 otherwise, i.e., a uniform kernel. The weights are normalized so that $\sum w_{x_g,x} = 1$. By principle, estimation is restricted to focal points where $N_{x_g}(\sqrt{2}l) \neq 0$.

B. Local multifractal analysis

In the following, C_1^i and $\rho_{ss}(x_g, r)$ will be computed with the multiscale coefficient $P^i(x, r)$ whilst C_2^i and $\rho_{mf}(x_g, r)$ with the wavelet p-leader $Q^i(x, r)$. Note that in a bivariate context, the two processes $(T^1(x, r)$ and $T^2(x, r))$ under analysis must reside on - or be antecedently projected to - a common set of points. To perform the local multifractal analysis, we need first to assess the local scaling for each component $i = 1, 2$:

$$\begin{aligned} C_1^i(x_g, r) &\sim c_1^i(x_g)\log(|r|) + d_1^i(x_g) \\ C_2^i(x_g, r) &\sim -c_2^i(x_g)\log(|r|) + d_2^i(x_g) \end{aligned} \tag{5}$$

This provides the local univariate multifractal analysis through the summary (c_1^i, c_2^i) for each component i. For the bivariate extension, to assess classical cross-correlation, we define the classical cross-coherence function of r, with $\overline{T}^i(x, r) = \sum_x w_{g,e} T^i(x, r)$, as:

$$\rho_{ss}(x_g, r) = \frac{\sum_x w_{x_g,x} T^1(x,r) T^2(x,r) - \overline{T}^1(x,r)\overline{T}^2(x,r)}{\sqrt{\left(\sum_x w_{x_g,x} T^1(x,r)^2\right)\left(\sum_x w_{x_g,x} T^2(x,r)^2\right)}} \tag{6}$$

In addition, following [9]–[11], to determine cross multifractality at the local level, we compute a multifractal coherence function of r:

$$\rho_{mf}(x_g, r) = \frac{C_1^{1,2}(x_g, r)}{\sqrt{C_2^1(x_g, r) C_2^2(x_g, r)}}. \tag{7}$$

with

$$\begin{aligned} C_1^{1,2}(x_g, r) &= \sum_x w_{x_g,x} \log|T^1(x, r)| \log|T^2(x, r)| \\ &- C_1^1(x_g, r) C_1^2(x_g, r) \end{aligned} \tag{8}$$

Analogously to the local scaling functions of the univariate option, these quantities are evaluated at every estimation site x_g for consecutive radii r. Specifically, ρ_{ss} measures a collection of scale-dependent local Pearson correlation coefficients amongst components of the data. Additionally, ρ_{mf} quantifies the cross-dependencies in the fluctuations of local regularities amongst components. When ρ_{mf} goes to 1, locally around a location, this indicates that both components are locally and jointly irregular and bursty. Finally, to evaluate global scaling characteristics, sums are performed across the sites x_g:

$$\begin{aligned} \overline{C_1^i(r)} = \frac{1}{N_{x_g}} \sum_{x_g} C_1^i(x_g, r) &\sim c_1^i \log(|r|) + d_1^i \\ \overline{C_2^i(r)} = \frac{1}{N_{x_g}} \sum_{x_g} C_2^i(x_g, r) &\sim -c_2^i \log(|r|) + d_2^i. \end{aligned} \tag{9}$$

IV. Results on three distinct point distributions

The aim of this section is twofold: first, to test if the above local multifractal analysis can recover globally prescribed multifractal parameters, and second, to validate how far local multifractal estimations depend on their underlying spatial point distributions.

A. Construction of non-homogenous bivariate point processes

Two essential steps are required to construct the bivariate marked point processes of interest here.

Multifractal random walk. First, numerical simulations are carried out with the help of a so-called multifractal random walk (MRW) [17], [18]. MRW is a well-known multiplicative cascade process whose multifractal properties are those of the multiplicative log-normal cascade of Mandelbrot.

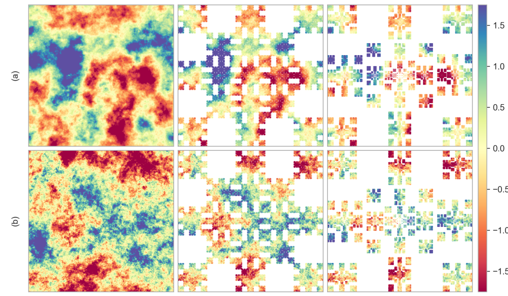

Fig. 1. The bivariate MRW process on a 2048*x*2048 grid with parameters $(H^1, H^2, c_2^1, c_2^2) = (0.7, 0.3, 0.05, 0.025)$, superposed on a homogenous raster grid *HG* (left), and on two non-homogeneous Sierpinski carpets: *S1* (center) and *S2* (right). The top row (**a**) shows the first (H^1, c_2^1) the bottom row (**b**) the second (H^2, c_2^2) component.

The *two-dimensional* bivariate MRW field is obtained as [19], [20]

$$m = 1, 2, X_m(\underline{x}) = G_m(\underline{x}) e^{\omega_m(\underline{x})} \tag{10}$$

where $\underline{x}$ are cartesian coordinates and $\underline{G}(\underline{x}) = \{G_1(\underline{x}), G_2(\underline{x})\}$, $\underline{\omega}(\underline{x}) = \{\omega_1(\underline{x}), \omega_2(\underline{x})\}$ are two independent pairs of stochastic processes with predefined covariance functions. $\underline{G}(\underline{x})$ is delineated as a 2D fractional Gaussian noise while the $\underline{\omega}(\underline{x})$ process is defined via 2×2 cross-covariance functions, to motivate multifractality in the spatial statistics [19]. Detailed expressions of the covariance functions can be found in [19], [20]. The MRW is then defined as a fractional integration of order one of $X_m(\underline{x})$. For the present work, it suffices to know that the self-similar cross-coherence function $\rho_{ss}(x_g, r)$ can be interpreted as the correlation ρ_G between the two processes $G_1(\underline{x})$ and $G_2(\underline{x})$. At the same time, $\rho_{mf}(x_g, r)$ is defined as the combination of the two correlations ρ_G and ρ_ω.

A mono- and multifractal point process. Secondly, to further illustrate general applicability that is valid for a wide range of 2D distributions, we construct two non-homogenous Sierpinski carpets - hereafter referred to as *S1* and *S2* - using the IFS fractal generator "GenFrac" [21]. Thereby, we deploy a single (*S1*, $d_0 = 1.76$) and then four different (*S2*, $d_0 = 1.56$) reduction factors to obtain a mono- and multifractal structure, respectively, with various local dimensions $d_0 = -\log(N_r)/\log(r)$. As our approach may be relevant for research on geographical systems, it is interesting to analyze such distinct distributions: *S1* is characterized by a relatively low (e.g., urban centers) and *S2* by a high variation in point densities (e.g., suburban or rural areas).

For this paper, we generate ten realizations of an MRW ($N = 2048$) [19] with parameters H^i and c_2^i using eq. 10. Going on, the MRW image - residing on a homogenous grid support (*HG*) - is defined as a marked point process with spatial positions in $[0,\ N-1]^2$. Moreover, the MRW values ("marks") are superposed on the different point patterns S1 and S2 at the respective rounded point location of their centroids. We obtain six marked point processes $\Gamma^{i,j} = x_{i,j}, y_{i,j}, \kappa_{i,j}$, $i = 1, 2$ (bivariate MRW) and $j = 1, 2, 3$ (supports *HG*, *S1*, *S2*). Figure 1 shows their support structure and the assigned MRW "mark" generated with $H^1 = 0.7$, $H^2 = 0.3$, and $c_2^1 = 0.05$,

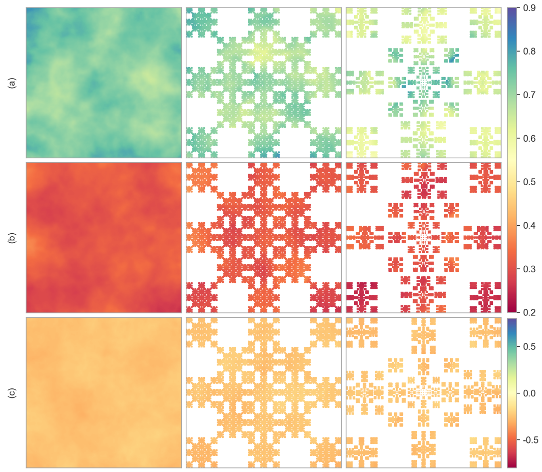

Fig. 2. **(a, b)** *Univariate* analysis. $c_1(x_g)$ (eq. 3 and 5) obtained on *HG* (left), *S1* (middle), and *S2* (right). The parameters used to generate the MRW process are $H^1 = 0.7$, $c_2^1 = 0.05$ (a) and $H^2 = 0.3$, $c_2^2 = 0.025$ (b). **(c)** *Bivariate* analysis. Results for the local cross-correlation coefficients $\rho_{ss}(x_g, r)$ (eq. 6).

$c_2^2 = 0.025$. Note that, mathematically, restricting an irregular process, such as increments of an MRW on a fractal set, can be ill-defined. However, this problem does not arise here because modeling is performed at a finite scale.

B. Performance assessment

For this analysis, the fourteen observed scales r are logarithmically spaced between $r = 2^4$ and 2^8 and $L = 280px$. Increasing the size of the local neighborhood L to reach the full image resolution ($2048x2048$) would yield results equivalent to that of the global analysis defined in eq. 9. Note that all results in this section are obtained as the mean across ten MRW realizations. Let us start by inspecting the analysis results of the two MRW fields independently. Figure 2 (a,b) displays the slope $c_1(x_g)$ of the fit for cumulant one $C_1^i(x_g, r)$ for every estimation site x_g. What stands out is the rather distinct color range of the two rows: brighter green color or higher exponents $c_1(x_g)$ dominating the top, and darker red patches, thus lower $c_1(x_g)$ values at the bottom. This indicates

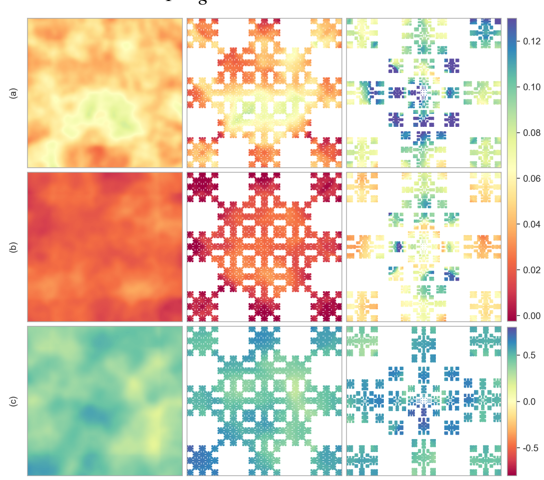

Fig. 3. **(a, b)** *Univariate* analysis. Analysis results for $c_2(x_g)$ (eq. 4 and 5) on the *HG* (left), *S1* (middle), and *S2* (right) support. Prescribed parameters are $H^1 = 0.7$, $c_2^1 = 0.05$ (a) and $H^2 = 0.3$, $c_2^2 = 0.025$ (b). **(c)** *Bivariate* analysis. Results for $\rho_{mf}(x_g, r)$ (eq. 7) estimations.

that globally assigned H exponents ($H^1 = 0.7$, $H^2 = 0.3$) can also be retraced locally. Figure 3 reveals similar tendencies, whereby lighter orange colors or higher intermittency ($c_2(x_g)$) dominates examples of the top row. Note that the appearance of these images can be perceived as rather *uniform*. MRW is an intermittent but statistically homogeneous field; therefore, we do not expect significant fluctuations in the local estimations of H^i and c_2^i. The followings assess estimation performance for the different multifractal parameters separately: *(i.)* In the case of $c_1(x_g)$, local regression quality is very good for all analyzed point processes: The coefficient of determination R^2 remains above 0.98 for all estimation sites on average. Moreover, in Figure 4, the histograms of the three $c_1(x_g)$ estimations (*HG, S1, S2*) are layered upon one another and peak at the prescribed H^i, signaling that results do not depend markedly on the supports. *(ii.)* Although the estimation quality degrades for $c_2(x_g)$, in the case of *HG* and *S1*, the derived values oscillate around the predefined c_2^2 in Figure 4.b. It is solely for the rather extreme spatial distribution of *S2* that results are somewhat skewed, and the intermittency of the MRW is overestimated. *(iii.)* Finally, cross-correlation coefficients in Figure 2.c and Figure 3.c (mean value across radii r) also confirm that local results are in accordance with predefined parameters: Values of the classical cross-correlation function using the multi-resolution coefficient $T^i(x, r)$ fluctuate in the close vicinity of $\rho_{ss} = -0.3$ and that of the multifractal cross-dependency - obtained with the help of $Q^i(x, r)$ - around the prescribed $\rho_{mf} = 0.5$. Similar to the univariate case, bivariate estimations also appear largely independent of the support in Figure 4.c, where the three respective histograms are positioned closely.

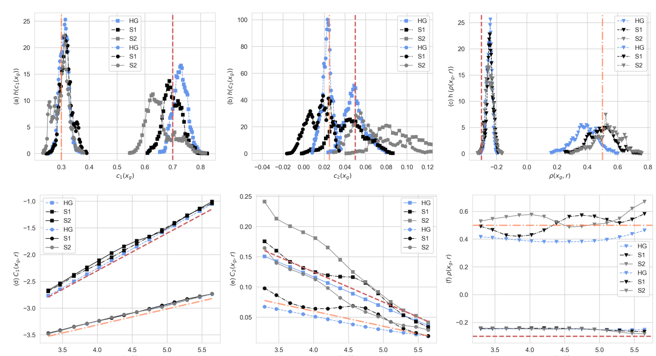

Fig. 4. In all subfigures, results (mean value across ten MRW realizations) are obtained on the three supports, *HG* (blue), *S1* (black), *S2* (grey), and the two MRW components (■ and •). The predefined MRW parameters are indicated in red ($i = 1$) and orange ($i = 2$) colors in the first two columns. The top row shows the histogram of the local scaling $c_1(x_g)$ **(a)** and $c_2(x_g)$ **(b)** according to eq. 5. In subfigure **(c)**, the histogram of local cross-correlations (mean value across all available scales) $\rho_{ss}(x_g, r)$ (eq. 6, the prescribed value is shown in red) and $\rho_{mf}(x_g, r)$ (eq. 7, orange) are displayed. Global scaling functions (eq. 9) are depicted in the second row (subfigures **d**,**e**,**f**).

In conclusion, all predefined MRW parameters can be correctly recovered for the homogenous grid *HG*. The non-homogenous point distribution of the first Sierpinski carpet *S1* does not seem to significantly alter any of the *local estimations* ($c_1(x_g)$, $c_2(x_g)$, $\rho_{ss}(x_g, r)$, $\rho_{mf}(x_g, r)$) compared to those obtained on *HG*. The immensely sparse bits of the second carpet $S2$ (Fig. 3 (a,b)), however, bias local intermittency $c_2(x_g)$ estimations of the MRW components. Notwithstanding, the bottom row of Figure 4 unequivocally demonstrates that both univariate and bivariate estimations for the three different supports are *concurrent on the global level*; The evolution of global scaling functions $\overline{C_1^i(r)}$, $\overline{C_2^i(r)}$ and $\overline{\rho_{ss}(r)}$, $\overline{\rho_{mf}(r)}$ (see eq. 9) for the three distributions are roughly by one another and with the progression of the theoretical lines colored in red and orange.

V. Applications in the Geospatial Context

Geospatial analysis and modeling frequently demand a multivariate and multiscale framework. Geographical data can also be regarded as a marked point process [13] whose spatial distribution is heterogeneous. Therefore, we contend that the proposed methodology may find essential applications amongst others in human, environmental, or economic geography. For example, prior studies have already linked the multifractality of socioeconomic variables to classical measures of inequality and segregation [4], [5]. Therefore it is compelling to observe if a bivariate multifractal analysis of, e.g., the ratio of under-18 and over-65-year-olds (in 2015 [22]) in the Paris metropolitan region may provide interesting insights. Note that in the case of our real-world example, performing a "local" analysis is of elevated relevance: As an example, for the entire 2D field of over-65-year-olds, the standard deviation ($\sigma_{c_i(x_g)}$) of $c_1(x_g)$ estimations is $\sigma_{c_1(x_g)} = 0.505$ while for the first and second MRW components, it is only $\sigma_{c_1^1(x_g)} = 0.036$ and $\sigma_{c_1^2(x_g)} = 0.027$. We find similar results for $c_2(x_g)$ and the bivariate parameters. Figure 5 shows the local cross-coherence functions ρ_{ss} and ρ_{mf}: These generally reveal the correlation between the multiscale spatial dependencies of these two demographic variables. The results indicate that the intensity and variability of the multifractal cross-correlation ρ_{mf} are more substantial than its self-similar counterpart ρ_{ss}. For instance, within the Petit-Couronne area, ρ_{mf} often displays large negative values. The latter signals rather extreme demographic differences on the neighborhood level, where one variable exhibits high local intermittency while the other is non-intermittent. It may be above all in these areas that current demographic trends contribute to an increase in small-scale societal polarization and may, therefore, swiftly necessitate various targeted mitigation measures.

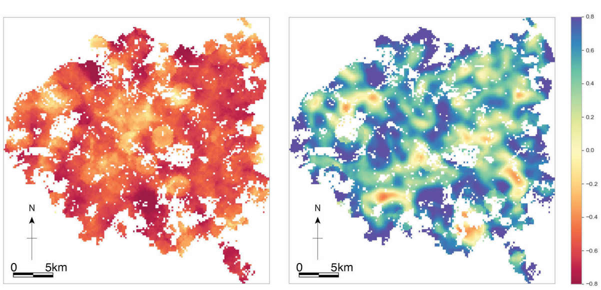

Fig. 5. Local multifractal cross-correlations coefficients ρ_{ss} (left) and ρ_{mf} (right) - mean value across all available scales - in and around the city of Paris ("Petite Couronne"), France. The bivariate data analyzed here consists of the ratio of under-18 and over-65-year-olds in 2015 [22].

Acknowledgment

Work supported by Projet Multifrac within the larger research framework I-SITE FUTURE of Université Gustave Eiffel (UGE) in France.

References

[1] P. Frankhauser, C. Tannier, G. Vuidel, & H. Houot (2018). "An integrated multifractal modeling to urban and regional planning". Computers, Environment and Urban Systems, 67, 132-146.
[2] F. Sémécurbe, C. Tannier and S. G. Roux (2019). "Applying two fractal methods to characterize the local and global deviations from scale invariance of built patterns throughout mainland France". Journal of Geographical Systems, 21(2), 271-293.
[3] J. Lengyel, S. G. Roux, F. Sémécurbe, S. Jaffard, P. Abry (2022). "Roughness and intermittency within metropolitan regions - Application in three French conurbations". Environment and Planning B: Urban Analytics and City Science, SAGE.
[4] J. Lengyel, S.G. Roux, P. Abry, F. Sémécurbe and S. Jaffard, (2022). "Local multifractality in urban systems—the case study of housing prices in the greater Paris region". Journal of Physics: Complexity, 3(4), p.045005.
[5] H. Salat, R. Murcio, K. Yano, & E. Arcaute (2018). "Uncovering inequality through multifractality of land prices: 1912 and contemporary Kyoto". PloS one, 13(4), e0196737.
[6] S. G. Roux, A. Arneodo and N. Decoster. "A wavelet-based method for multifractal image analysis. III. Applications to high-resolution satellite images of cloud structure." The European Physical Journal B-Condensed Matter and Complex Systems 15.4 (2000): 765-786.
[7] C. Meneveau, K. Sreenivasan, P. Kailasnath, M. Fan, "Joint multifractal measures — theory and applications to turbulence", Phys. Rev. A 41 (2) (1990) 894–913.
[8] J. Peyrière, "A vectorial multifractal formalism, Proc. Sympos". Pure Math. 72 (2) (2004) 217–230.
[9] S. Jaffard, S. Seuret, H. Wendt, R. Leonarduzzi, S. Roux, and P. Abry, (2019). "Multivariate multifractal analysis". Applied and Computational Harmonic Analysis, 46(3), 653–663.
[10] H. Wendt, R. Leonarduzzi, P. Abry, S. Roux, S. Jaffard and S. Seuret, "Assessing Cross-Dependencies Using Bivariate Multifractal Analysis," 2018 IEEE International Conference on Acoustics, Speech and Signal Processing (ICASSP), 2018, pp. 4514-4518, doi: 10.1109/ICASSP.2018.8461752.
[11] S. Jaffard, S. Seuret, H. Wendt, R. Leonarduzzi, and P. Abry, (2019). "Multifractal formalisms for multivariate analysis". Proceedings of the Royal Society A, 475(2229), 20190150.
[12] H. Wendt, S. Combrexelle, Y. Altmann, J. Y. Tourneret, S. McLaughlin, & P. Abry, (2018). "Multifractal analysis of multivariate images using gamma Markov random field priors". SIAM Journal on Imaging Sciences, 11(2), 1294-1316.
[13] J. Illian, A. Penttinen, H. Stoyan, & D. Stoyan, (2008). "Statistical analysis and modeling of spatial point patterns" (Vol. 70). Wiley&Sons.
[14] LomPy. URL: https://pypi.org/project/lompy/
[15] J. F. Muzy, E. Bacry, & A. Arneodo (1993). "Multifractal formalism for fractal signals: The structure-function approach versus the wavelet-transform modulus-maxima method". Physical Review E, 47(2), 875.
[16] R. Leonarduzzi, H. Wendt, P. Abry, S. Jaffard, C. Melot, S. G. Roux, & M. E. Torres (2016). "p-exponent and p-leaders, Part II: Multifractal analysis. Relations to detrended fluctuation analysis". Physica A: Statistical Mechanics and its Applications, 448, 319-339.
[17] E. Bacry, J. Delour, & J. F. Muzy, (2001). "Multifractal random walk". Physical Review E, 64(2), 026103.
[18] J. F. Muzy, & E. Bacry, (2002). "Multifractal stationary random measures and multifractal random walks with log infinitely divisible scaling laws". Physical Review E, 66(5), 056121.
[19] P. Abry, V. Mauduit, E. Quemener, & S. Roux, (2022). "Multivariate multifractal texture DCGAN synthesis: How well does it work? How does one know?". Journal of Signal Processing Systems, 1-17.
[20] Leonarduzzi, R., Abry, P., Roux, S., Wendt, H., Jaffard, S., Seuret, S. (2018, September). Multifractal characterization for bivariate data. In 2018 26th European Signal Processing Conference (EUSIPCO) (pp. 1347-1351). IEEE.
[21] GenFrac, Fractal Generator. URL: https://sourcesup.renater.fr/www/genfrac/.
[22] INSEE. URL: https://www.insee.fr/fr/statistiques/.